Chapter 6
Energy harvesting in pumping cycle operation

Roland Schmehl

Abstract The objective is to develop a performance model for crosswind airborne wind energy systems in pumping cycle operation. The model combines the two idealized quasi-steady flight states originally introduced by Loyd: crosswind flight for the power-generating reel-out phase and tether-aligned descent for the power-consuming reel-in phase. Transitions between the two states and the gravitational effect of kite mass are not taken into account. Following Luchsinger, the cycle power is maximized by optimizing the reeling speeds while accounting for two system-specific hardware constraints. For low wind speeds, the kite operation is unconstrained, and both reeling speeds are optimized. For medium wind speeds, the tether force during reel-out is limited by increasing the reel-out speed with the wind speed. For high wind speeds, the generator power during reel-out must also be limited by increasingly depowering the kite with the wind speed. The developed optimization strategies for the three wind speed regimes allow the prediction of an achievable power curve from a few key design parameters of the system.

Roland Schmehl (✉)
Delft University of Technology, Faculty of Aerospace Engineering, Kluyverweg 1, 2629 HS Delft, The Netherlands
e-mail: r.schmehl@tudelft.nl

6.1 Introduction

Airborne wind energy systems based on pumping cycle operation have emerged as a dominant industry choice for implemented prototypes with power ratings up to several hundred kilowatts. While kites vary from soft-wing to hybrid and fixed-wing types with respectively tailored launch and landing concepts, crosswind flight operation during reel-out is the common key feature for increasing the tether force and power output. In his seminal paper, Loyd (1980) compared the maximum achievable power when flying crosswind maneuvers to the power when not flying maneuvers. The idealized analysis showed that crosswind flight with a reasonably high lift-to-drag ratio (≈ 15) amplifies the power output theoretically by two orders of magnitude. This finding triggered the exploration of pumping cycle operation for harvesting wind energy, flying crosswind maneuvers during reel-out and discontinuing the maneuvers during reel-in. Because of the characteristic reel-out and reel-in motion, this mode of operation is frequently dubbed as yo-yo concept.

Terink (2009) expanded on Loyd's theory to derive the tractive power in the two alternating phases using representative quasi-steady flight states, accounting for the effects of an elevation angle but neglecting the effect of gravity. He combined the analytic expressions to calculate the net cycle power, not considering hardware limits and optimization of operational parameters. Luchsinger (2013) introduced tether force and generator power limits of real systems, adding control and optimization strategies to maximize the net power output while ensuring that the hardware limits are respected over the entire wind speed range. The underlying model also uses two representative quasi-steady flight states and neglects the effect of gravity. Setting the elevation angle during reel-in to the angle during reel-out requires a very low lift component during reel-in. Such a condition can only be realized with fixed-wing systems because soft-wing systems require a non-zero lift component to maintain structural stability. Fechner and Schmehl (2013) proposed a similar modeling approach tailored to soft-wing systems, determining the reel-in flight path by numerical integration while also optimizing the reel-in speed. Schelbergen et al. (2020) used the quasi-steady model of Schmehl et al. (2013) and Van der Vlugt et al. (2019)

The framework was first presented in Schmehl et al. (2024) for applications on Mars.

The lecture notes are structured as follows. The working principle and concept of operations of the considered pumping kite power system are outlined in Sect. 6.2, followed by a discussion of kite kinematics and key assumptions in Sect. 6.3. In Sect. 6.4, an analytical model is developed accounting for the reel-out and reel-in phases of the pumping cycle and the different aerodynamic loads, reeling speeds, and time durations. In Sect. 6.5, the conversion model is used for systematic optimization of the operational parameters, distinguishing three wind speed regimes with different operational strategies. The control concept was introduced by Luchsinger (2013) and Fechner and Schmehl (2013) to account for constraints of a real implemented system. In Sect. 6.6, additional conversion losses are incorporated in the model, as proposed by Fechner and Schmehl (2013), to determine in Sect. 6.7 the net electrical power output of the system per production cycle, day and year.

6.2 Working principle and concept of operations

The general working principle of an AWE system operated in pumping cycles is illustrated in Fig. 6.1. The diagram depicts a representative cycle trajectory in the

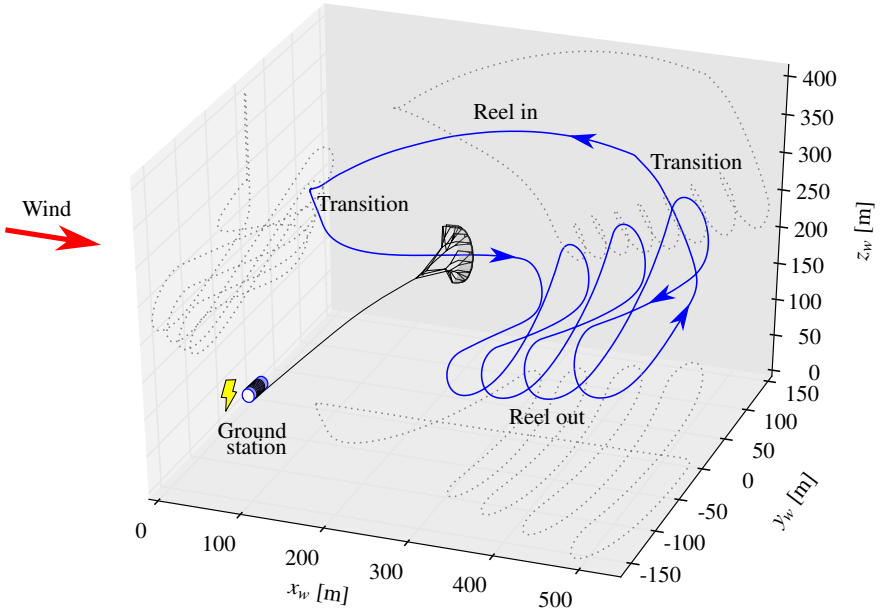

Fig. 6.1: Flight path of a soft-kite based pumping AWE system computed in the wind reference frame with a dynamic system model (adapted from Fechner 2016). Kite and drum not to scale.

wind reference frame, spanned by the x_w-, y_w- and z_w-axes. The origin of this reference frame is located at the point where the tether exits from the ground station's drum, the x_w-axis is pointing in the direction of the wind, and the z_w-axis vertically upwards (Schmehl et al. 2013).

During the reel-out phase, the kite is operated in crosswind maneuvers, in the illustrated case, consecutive figure-of-eight patterns, maximizing the pulling force and thus also the generated energy. In the literature, this phase is also denoted as the traction or production phase. When reaching the maximum deployed tether length, the crosswind maneuvers are terminated, and the kite is depowered and steered into the $x_w z_w$-plane. To depower the kite, its rear bridle lines are released such that the wing pitches forward to a lower angle of attack with the relative flow. This substantially decreases the aerodynamic forces. In this outer transition phase, the tether is kept at a constant length while the kite flies towards the z_w-axis continuously increasing its elevation angle. Before reaching the $x_w z_w$-plane and a static flight state, the ground station generally starts to reel in the tether.

During the reel-in phase, energy is consumed because the drum works against the pulling force of the kite, which is much lower than in the reel-out phase but still required to keep the airborne system under tension. In the literature, this phase is also denoted as the retraction or consumption phase. For the same reasons of structural stability, a soft-kite-based system can only be depowered to a certain degree. Consequently, the aerodynamic lift-to-drag ratio is still relatively high, which leads to a continuous increase in the elevation angle when reeling in. This process is also used for winch launching a kite from the ground or step towing to keep the kite airborne despite a too-low wind speed. When reaching the minimum deployed tether length, the kite is powered again by pulling in the rear bridle lines. In this inner transition phase, the tether is kept at a constant length while the kite flies towards the x_w-axis, continuously decreasing its elevation angle. Before reaching a static flight state, the crosswind maneuvers are reinitiated, and the ground station starts to reel out the tether, starting the next pumping cycle.

The net generated energy per cycle is the difference between the energy generated in the reel-out phase and the energy consumed in the reel-in phase. This latter amount of energy has to be stored suitably during the reel-out phase. Most currently implemented smaller-scale systems use rechargeable batteries or supercapacitors, while other options, such as hydraulic drivetrains with pneumatic storage, might be of interest for larger-scale implementations (Hagen et al. 2023). In practice, the transition phases are generally kept as short as possible to minimize the associated losses in net power. For a soft-wing kite system, the depowering and powering of the wing takes a few seconds and is blended into the reel-in and reel-out phases.

During the reel-in phase and the two transition phases, the flight control system aims to keep the flight motion of the kite within the $x_w z_w$-plane, such that the flight path is roughly two-dimensional. During the reel-out phase, the kite is steered along three-dimensional, outgoing figure-of-eight maneuvers. In contrast to a wind turbine, pumping crosswind AWE systems thus harvest from a larger volume of the atmosphere.

Launching and landing do not contribute to energy harvesting but are indispensable operational phases to start up and shut down the pumping cycle operation. For example, when a thunderstorm approaches or other hazardous conditions are foreseeable, the kite must be landed, secured, and stored safely before it can eventually be launched again. Similarly, when the wind speed drops below the cut-in wind speed for an extended time period, the kite has to be landed and relaunched once the wind picks up again. For shorter periods, the kite can be kept airborne using the energy-consuming technique of step towing.

More details about the concept of operations are provided in Van der Vlugt et al. (2013), Van der Vlugt et al. (2019) and Salma et al. (2019).

6.3 Kite kinematics and key assumptions

The control system of the AWE system governs two distinctly different motion components of the kite. The component along the tether is imposed by the reeling speed of the ground station. The component in the plane perpendicular to the tether can be described by a flight direction and speed. The direction is controlled by the steering mechanism of the kite control unit. On the other hand, the flight speed cannot be controlled directly because a kite does not have a propulsion system. Instead, it is influenced by several factors, among others, the aerodynamic characteristics of the kite, most importantly the lift-to-drag ratio, the reeling speed, and the degree of alignment of flight direction and gravitational acceleration. The strong aerodynamic coupling of the two orthogonal motion components and the dominant effect of the flight speed on the pulling force explains why reliable and robust control of a kite in a varying and fluctuating wind environment still constitutes a challenge for the commercial development of AWE systems.

The described control concept and kinematic decomposition are applicable during flight phases of constant tether sag. Since the tether shape is determined by the equilibrium of the distributed load along the tether, such as aerodynamic drag, gravity, centrifugal acceleration, and the tether forces at both ends, sudden changes in these contributions also affect the tether sag. A changing sag, in turn, leads to a rotation of the kite with respect to the ground station. This can be observed, for example, when powering or depowering the kite or when starting or stopping crosswind maneuvers.

Figure 6.2 illustrates the different tether geometries during reel out and reel in. While the tether is practically straight when flying crosswind maneuvers during reel-

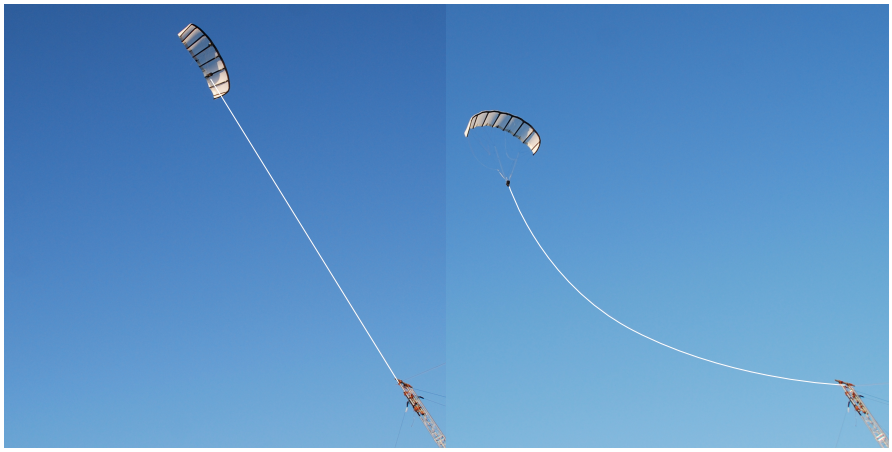

Fig. 6.2: Kite performing crosswind flight maneuvers with practically straight tether while reeling out (left) and non-maneuvering kite with strongly sagging tether while reeling in (right). Photographic footage with traced tether from 2 August 2012.

out, this particular flight test shows a rather extreme tether sag during reel-in, mainly because of low wind and reel-in speeds leading to a relatively low tether force. It should be noted that the photos do not depict the regular pumping cycle operation of the kite but the launching and landing phases with a relatively short deployed tether length, using an experimental setup with a tilted mast (Van der Vlugt et al. 2019; Salma et al. 2019).

A simplified mathematical model of tethered flight and tractive power generation can be derived by assuming a straight and inelastic tether. Using spherical coordinates (r, ϕ, β), the position of the kite in the wind reference frame can be described by the radial distance r of the kite from the ground station, which is identical to the deployed tether length l_t, the azimuth angle ϕ measured from the $x_\mathrm{w}z_\mathrm{w}$-plane, and the elevation angle β measured from the ground plane. The flight velocity $\mathbf{v}_\mathrm{k}$ of the kite can be described by radial and tangential components $\mathbf{v}_\mathrm{k,r}$ and $\mathbf{v}_{\mathrm{k},\tau}$, respectively. The radial speed $v_\mathrm{k,r}$ is identical to the reeling speed v_t of the tether. It is positive for reel-out and negative for reel-in. The tangential velocity component is defined by the speed $v_{\mathrm{k},\tau}$ and the course angle χ, measured in the local tangential plane τ from a defined reference direction. By definition, the tangential speed $v_{\mathrm{k},\tau}$ can not be negative (Schmehl et al. 2013).

Figure 6.3 illustrates the definition of the kite's position and velocity in spherical coordinates. The magnitudes of the radial and tangential components of the flight

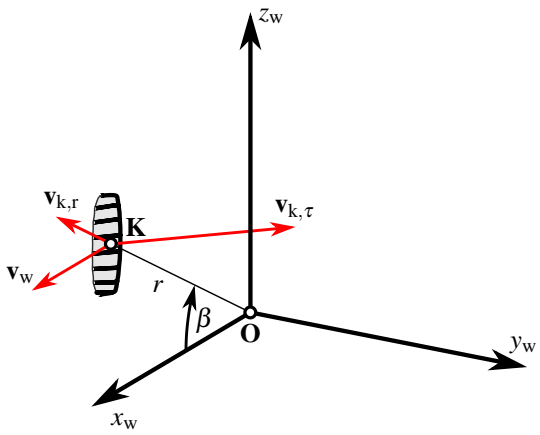

Fig. 6.3: Kite with an idealized straight tether of variable length r at elevation angle β for the special case of the kite just passing through the $x_\mathrm{w}z_\mathrm{w}$-plane ($\phi = 0$).

velocity can be nondimensionalized with the wind speed,

$$\frac{v_\mathrm{k}}{v_\mathrm{w}} = \sqrt{f^2 + \lambda^2}, \tag{6.1}$$

$$f = \frac{v_\mathrm{k,r}}{v_\mathrm{w}} = \frac{v_\mathrm{t}}{v_\mathrm{w}}, \tag{6.2}$$

$$\lambda = \frac{v_{\mathrm{k},\tau}}{v_{\mathrm{w}}}, \tag{6.3}$$

introducing the reeling factor f and the tangential velocity factor λ.

Figure 6.4 shows a side view of the three-dimensional flight path depicted in Fig. 6.1. The pumping cycle evolves through six characteristic points in times,

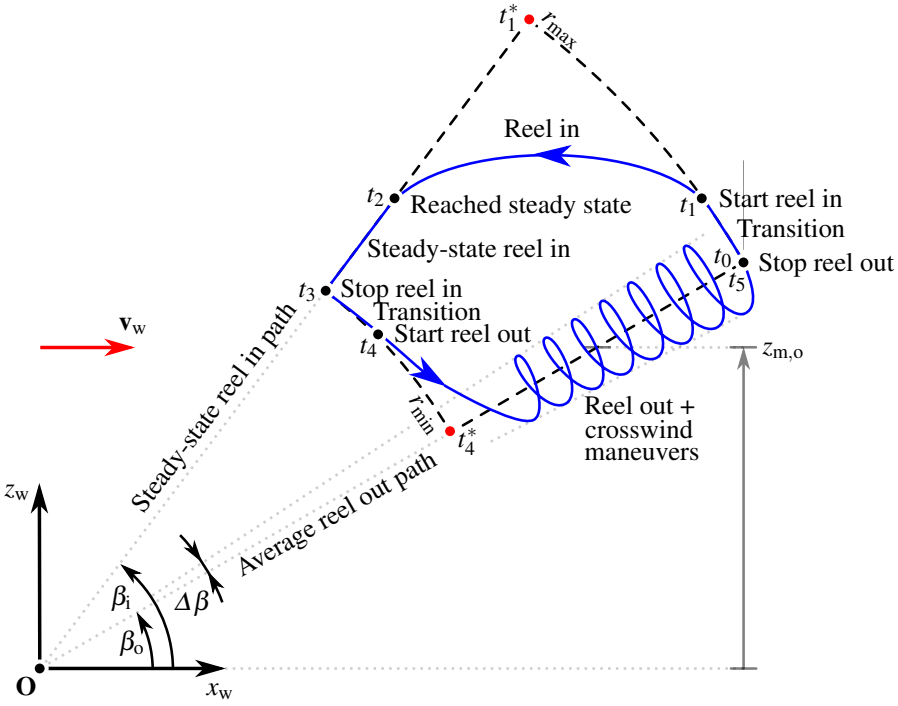

Fig. 6.4: Side view of real (solid blue) and idealized (dashed) flight paths.

$t_0 - t_1 - t_2 - t_3 - t_4 - t_5$. Following a convention introduced by Van der Vlugt et al. (2019), the start time t_0 of the cycle is set to the end of the reel-out phase. In this schematic, the angle β_{o} describes the average elevation angle during reel out with the nondimensional speed f_{o}, while the angle β_{i} describes the constant elevation angle during steady-state reel in with the constant nondimensional speed f_{i}. It should be noted that this asymptotic limit state is not necessarily reached, as it is depicted in Fig. 6.4. Depending on the aerodynamic properties of the depowered kite, its mass, the reel-in speed, and the covered radial distance $r_{\max} - r_{\min}$, the reel-in phase may end at t_3 before reaching the steady-state flight condition with constant elevation angle β_{i}. The parameter $z_{\mathrm{m,o}}$ describes the mid-altitude of the reel-out phase, which will be used to evaluate the wind resource accessible for conversion.

Table 6.1 describes how the position and the nondimensional velocity variables vary along the phases of the pumping cycle. The first part of the reel-in phase is

Table 6.1: Phases of pumping cycle operation of a soft-wing kite.

Start time	Name	Kite position			Kite velocity		
		r	ϕ	β	f	λ	χ^{a}
t_0	Outer transition	$r_{\max}$	$\to 0$	$\nearrow$	0	>0	$\to 0$
t_1	Reel in	$\searrow$	≈ 0	$\nearrow$	$f_{\mathrm{i}}<0$	>0	≈ 0
t_2	Steady-state reel in	$\searrow$	≈ 0	β_{i}	$f_{\mathrm{i}}<0$	0	≈ 0
t_3	Inner transition	$r_{\min}$	≈ 0	$\searrow$	0	>0	$\to \pi$
t_4	Reel out	$\nearrow$	$\pm\Delta\phi$	$\beta_{\mathrm{o}}\pm\Delta\beta$	$f_{\mathrm{o}}>0$	$\gg 0$	$\pm\pi$
t_5	Outer transition	...					

[a] Course angle relative to the local upwards direction $\mathbf{e}_\beta$, as in Fechner and Schmehl (2018).

described by $\lambda > 0$ and increasing elevation angle β, while the second part of the steady-state reel-in is described by $\lambda = 0$ and constant elevation angle β_{i}.

To assess the generated and consumed energies over a pumping cycle, we need to identify one or more representative flight states for each phase and, from these, estimate the respective pulling force of the kite. The most basic approach uses one flight state for the reel-out phase and a separate one for the reel-in phase (Terink 2009; Luchsinger 2013). A suitable choice for the reel-out phase is a crosswind flight condition at the average elevation angle β_{o}, while for the reel-in phase, it is the steady flight state at the asymptotic limit angle β_{i}. The corresponding idealized flight path is included as a dashed line $t_0 - t_1^* - t_3 - t_4^* - t_5$ in Fig. 6.4. The approximation entails that the transition phases are infinitely fast, i.e., $t_1^* = t_0$ and $t_4^* = t_3$, such that the pumping cycle operation practically switches between reel-out and reel-in flight states. Because the transition phases are periods of zero power generation, they represent losses of net power. To maximize the cycle power, the transition phases will be shortened to a minimum feasible duration, which means that the approximation should be quite reasonable for any optimized commercial AWE system. In the next section, the two representative flight states will be used to estimate the net power over a pumping cycle.

Formulating the mathematical model in terms of nondimensional parameters f and λ defined by Eqs. (6.2) and (6.3) is important for investigating how airborne wind energy generation scales. However, in a realistic wind field, the wind speed varies in space and time. The question arises of which wind speed value is most suitable to characterize the energy conversion process. Given that the kite harvests wind energy over a large altitude range, the variation of the wind speed with altitude is important to consider. Because the power output of the reel-out phase is ruling for the net energy produced, the mid-altitude of this phase will be used, as suggested by Van der Vlugt et al. (2019) and indicated in Fig. 6.4

$$z_{\mathrm{m,o}} = \frac{1}{2}\left(r_{\min} + r_{\max}\right)\sin\beta_{\mathrm{o}}. \tag{6.4}$$

The tractive power of the kite is the product of the tether force and the reeling speed at the ground station. The dominant contribution to the tether force is the resultant aerodynamic force of the kite, commonly represented as a combination of lift and drag components

$$\mathbf{F}_\mathrm{a} = \mathbf{L} + \mathbf{D}, \qquad \text{with} \tag{6.5}$$

$$L = \frac{1}{2}\rho v_\mathrm{a}^2 C_\mathrm{L} S, \tag{6.6}$$

$$D = \frac{1}{2}\rho v_\mathrm{a}^2 \left(C_\mathrm{D,k} S + \frac{1}{4} C_\mathrm{D,t} d_\mathrm{t} r \right), \tag{6.7}$$

where ρ is the atmospheric density, C_L and $C_\mathrm{D,k}$ are the lift and drag coefficients, and S the planform area of the kite, respectively, $C_\mathrm{D,t}$ is the drag coefficient of a cylinder in a cross flow, and d_t is the tether diameter (Van der Vlugt et al. 2019). Equation (6.7) can be reformulated in terms of a lumped drag coefficient C_D

$$D = \frac{1}{2}\rho v_\mathrm{a}^2 C_\mathrm{D} S, \qquad \text{with} \tag{6.8}$$

$$C_\mathrm{D} = C_\mathrm{D,k} + \frac{1}{4} C_\mathrm{D,t} \frac{d_\mathrm{t} r}{S}. \tag{6.9}$$

Similarly to the argument presented for Eq. (6.4), we use in this approximation the mean tether length during the reel-out phase

$$r_\mathrm{m,o} = \frac{1}{2}\left(r_\mathrm{min} + r_\mathrm{max}\right). \tag{6.10}$$

By definition, the drag component $\mathbf{D}$ is aligned with the apparent wind velocity $\mathbf{v}_\mathrm{a}$ while the lift component $\mathbf{L}$ is perpendicular to it. The apparent wind velocity is defined as the relative flow velocity at the kite

$$\mathbf{v}_\mathrm{a} = \mathbf{v}_\mathrm{w} - \mathbf{v}_\mathrm{k}. \tag{6.11}$$

Inserting Eqs. (6.6) and (6.8) into Eq. (6.5) and making use of the orthogonality of the two force components, the magnitude of the aerodynamic force can be evaluated as

$$F_\mathrm{a} = \frac{1}{2}\rho C_\mathrm{L} \sqrt{1 + \frac{1}{E^2}} S v_\mathrm{a}^2, \tag{6.12}$$

where E denotes the lift to drag ratio L/D of the kite.

Because of the low mass and large wing surface area of membrane kites, inertial forces play only a minor role, and the kite's motion can be assumed to be quasi-steady. Furthermore, in the power production phase, the aerodynamic force is substantially larger than the gravitational force acting on the kite, and as a consequence, the tether force can be approximated by the tether force

$$0 = \mathbf{F}_\mathrm{t} + \mathbf{F}_\mathrm{a}. \tag{6.13}$$

Accordingly, the nondimensional tether force and tractive power can be derived as

$$\frac{F_\mathrm{t}}{qS} = C_\mathrm{L}\sqrt{1+\frac{1}{E^2}}\left(\frac{v_\mathrm{a}}{v_\mathrm{w}}\right)^2, \tag{6.14}$$

$$\zeta = \frac{P}{P_\mathrm{w}S} = C_\mathrm{L}\sqrt{1+\frac{1}{E^2}}f\left(\frac{v_\mathrm{a}}{v_\mathrm{w}}\right)^2, \tag{6.15}$$

where q denotes the dynamic wind pressure and P_w the wind power density,

$$q = \frac{1}{2}\rho v_\mathrm{w}^2, \tag{6.16}$$

$$P_\mathrm{w} = \frac{1}{2}\rho v_\mathrm{w}^3. \tag{6.17}$$

The nondimensional power ζ defined by Eq. (6.15) is also denoted as power harvesting factor (Diehl 2013; Schmehl et al. 2013; Vander Lind 2013).

6.4 Kite mechanical power generation

The net mechanical energy of a pumping cycle is the difference between the generated and consumed energies during the reel-out and reel-in phases, respectively. Applying the idealizations outlined in the previous section, these energies can be estimated with Eq. (6.15), using the wind power density P_w at the location, the planform area S and aerodynamic properties C_L and E of the kite, the reeling factor f and the nondimensional apparent wind speed $v_\mathrm{a}/v_\mathrm{w}$ in each cycle phase.

Apparent wind speed, tether force and mechanical power

A general expression for $v_\mathrm{a}/v_\mathrm{w}$ can be derived by decomposing the velocity vector into radial and tangential components,

$$\mathbf{v}_\mathrm{a} = \mathbf{v}_{\mathrm{a,r}} + \mathbf{v}_{\mathrm{a},\tau}, \tag{6.18}$$

and then, using the orthogonality of the components to formulate the velocity magnitude, as

$$\frac{v_\mathrm{a}}{v_\mathrm{w}} = \frac{v_\mathrm{a,r}}{v_\mathrm{w}}\sqrt{1+\left(\frac{v_{\mathrm{a},\tau}}{v_\mathrm{a,r}}\right)^2}. \tag{6.19}$$

The radial velocity component in this expression can be derived from the radial component of Eq. (6.11),

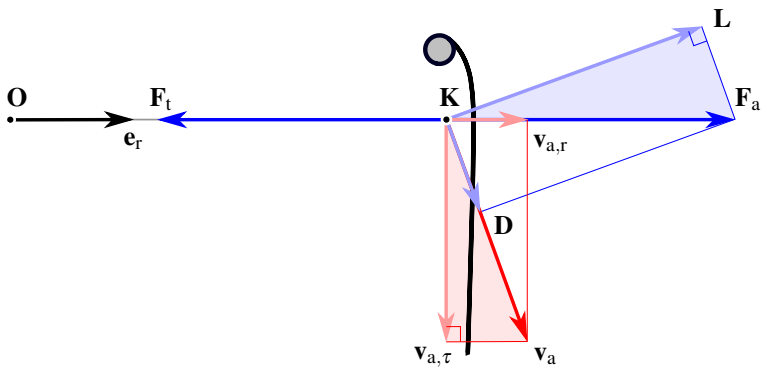

Fig. 6.5: Quasi-steady force equilibrium governing the flight motion of a massless kite, with apparent wind velocity components $\mathbf{v}_{a,\tau}$ and $\mathbf{v}_{a,r}$, and aerodynamic force components $\mathbf{L}$ and $\mathbf{D}$, in the plane spanned by the apparent wind velocity $\mathbf{v}_\mathrm{a}$ and the resultant aerodynamic force $\mathbf{F}_\mathrm{a}$.

$$v_{\mathrm{a,r}} = v_{\mathrm{w,r}} - v_{\mathrm{k,r}}, \tag{6.20}$$

substituting $v_{\mathrm{w,r}} = \cos\beta v_\mathrm{w}$, as illustrated in Fig. 6.3, and $v_{\mathrm{k,r}} = f v_\mathrm{w}$, according to Eq. (6.2), to get

$$\frac{v_{\mathrm{a,r}}}{v_\mathrm{w}} = \cos\beta - f. \tag{6.21}$$

This expression implies $\phi = 0$. For an arbitrary azimuth angle, an additional orthogonal projection into the $x_\mathrm{w}z_\mathrm{w}$-plane needs to be applied, multiplying $\cos\beta$ by $\cos\phi$ (Schmehl et al. 2013).

Assuming that the flight motion of the kite is governed by the quasi-steady equilibrium of the resultant aerodynamic force and the tether force only, it can be shown that the ratio $v_{\mathrm{a},\tau}/v_{\mathrm{a,r}}$ is identical to the lift-to-drag ratio of the kite (Schmehl et al. 2013)

$$\frac{v_{\mathrm{a},\tau}}{v_{\mathrm{a,r}}} = \frac{L}{D} = E. \tag{6.22}$$

This fundamental identity derives from the geometric similarity of the velocity and force triangles illustrated in Fig. 6.5. Because the vectors $\mathbf{v}_\mathrm{a}$ and $\mathbf{L}$ are perpendicular by definition, and the vectors $\mathbf{v}_{\mathrm{a},\tau}$ and $\mathbf{F}_\mathrm{a}$ are perpendicular by assumption of $\mathbf{F}_\mathrm{a} + \mathbf{F}_\mathrm{t} = 0$, and because the colored velocity and force triangles are right triangles, the two triangles are also geometrically similar.

Inserting Eqs. (6.21) and (6.22) into Eq. (6.19), leads to the following algebraic expression for the nondimensional apparent wind speed experienced by a kite flying in the $x_\mathrm{w}z_\mathrm{w}$-plane

$$\frac{v_\mathrm{a}}{v_\mathrm{w}} = \sqrt{1+E^2}\,(\cos\beta - f)\,, \tag{6.23}$$

describing the dependency on the operational parameters β and f and the design parameter E. The speed is unaffected by the flight direction, decreases with increasing

elevation angle and reeling factor, and increases with E. Inserting Eq. (6.23) into Eqs. (6.14) and (6.15) leads to

$$\frac{F_\mathrm{t}}{qS} = C_\mathrm{L}\sqrt{1+\frac{1}{E^2}}\left(1+E^2\right)(\cos\beta - f)^2\,, \tag{6.24}$$

$$\frac{P}{P_\mathrm{w}S} = C_\mathrm{L}\sqrt{1+\frac{1}{E^2}}\left(1+E^2\right)f\,(\cos\beta - f)^2\,, \tag{6.25}$$

During the reel-out phase, the kite is generally flown with a high lift-to-drag ratio to maximize the tether force and the generated power. In this case, for $E \gg 1$, Eqs. (6.23) to (6.25) further simplify to

$$\frac{v_\mathrm{a}}{v_\mathrm{w}} = E\,(\cos\beta - f)\,, \tag{6.26}$$

$$\frac{F_\mathrm{t}}{qS} = C_\mathrm{L}E^2\,(\cos\beta - f)^2\,, \tag{6.27}$$

$$\frac{P}{P_\mathrm{w}S} = C_\mathrm{L}E^2 f\,(\cos\beta - f)^2\,. \tag{6.28}$$

Equations (6.23) to (6.28) describe the relative flow velocity, tether force and tractive power of a massless kite in the $x_\mathrm{w}z_\mathrm{w}$-plane over the whole pumping cycle.

The ground station controls the reeling factor f. During crosswind flight, the tangential velocity factor λ adjusts to the instantaneous position and flight direction along the trajectory, depending on the kite's aerodynamic characteristics (Schmehl et al. 2013). During steady-state reel-in, the tangential motion component of the kite is zero. The aerodynamic characteristics of the kite are now a function of the reeling speed and the desired descent angle. This specific flight condition will be investigated in the following.

Reel-in phase

The situation during steady-state reel-in is depicted in Fig. 6.6. To descend with a constant elevation angle β, the kite velocity $\mathbf{v}_\mathrm{k}$ has to align with the tether. For this specific flight mode, Eq. (6.11) can be developed into an alternative algebraic expression for the nondimensional apparent wind speed

$$v_\mathrm{a}^2 = (v_\mathrm{w} + \cos\beta v_\mathrm{k})^2 + (\sin\beta v_\mathrm{k})^2\,, \tag{6.29}$$

$$= v_\mathrm{w}^2 + 2v_\mathrm{w}v_\mathrm{k}\cos\beta + v_\mathrm{k}^2, \tag{6.30}$$

$$\frac{v_\mathrm{a}}{v_\mathrm{w}} = \sqrt{1 - 2f\cos\beta + f^2}. \tag{6.31}$$

Equation (6.29) is constructed as a geometric relation assuming positive wind and kite speeds. The minus sign in Eq. (6.31) accounts for the negative value of f during reel-in. The above derivation is based solely on the kinematic requirement of align-

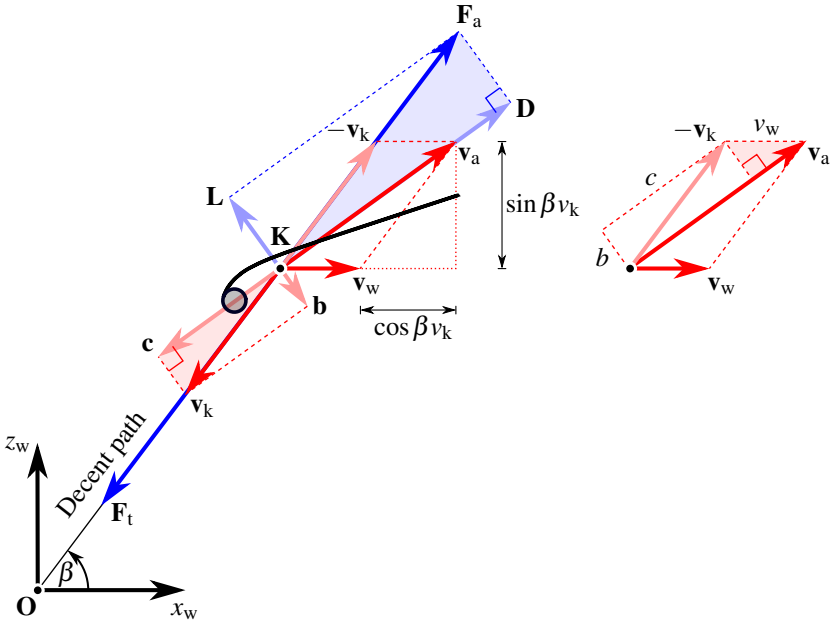

Fig. 6.6: Steady-state reel in of a massless kite at constant elevation angle β.

ing the kite velocity vector with the tether. Forces are not considered in this derivation. As seen from Fig. 6.6, the requirement of aligning the resultant aerodynamic force vector with the tether to satisfy the quasi-steady force equilibrium introduces a coupling of the lift and drag components. Consequently, a desired combination of descent path angle β and reeling factor f will require a specific lift-to-drag ratio E value. This relationship can be derived formally following Loyd's theory for the simple (non-crosswind) kite, adapted for the case of reeling in the tether.

As illustrated in Fig. 6.6, the kite velocity $\mathbf{v}_k$ can be decomposed into components $\mathbf{c}$ and $\mathbf{b}$ aligned with and perpendicular to the apparent wind velocity. Using these to substitute $\mathbf{v}_a$ in Eq. (6.11) gives

$$\mathbf{v}_a = \mathbf{v}_w - \mathbf{b} - \mathbf{c}, \tag{6.32}$$

$$v_w^2 = (v_a - c)^2 + b^2, \tag{6.33}$$

where we again assume that c and b are positive speeds. Equation (6.33) is visualized in Fig. 6.6 by the colored triangle included in the right-hand side detail. Considering then the geometric similarity of the colored velocity and force triangles on the left-hand side of Fig. 6.6, we can derive the following relations

$$\frac{b}{v_k} = \frac{L}{F_a} = \frac{1}{\sqrt{1+\frac{1}{E^2}}}, \tag{6.34}$$

$$\frac{c}{v_\mathrm{k}} = \frac{D}{F_\mathrm{a}} = \frac{1}{\sqrt{1+E^2}}, \tag{6.35}$$

which are further normalized to the wind speed to

$$\frac{b}{v_\mathrm{w}} = -\frac{f}{\sqrt{1+\frac{1}{E^2}}}, \tag{6.36}$$

$$\frac{c}{v_\mathrm{w}} = -\frac{f}{\sqrt{1+E^2}}. \tag{6.37}$$

As in Eq. (6.31), the minus signs in Eqs. (6.36) and (6.37) account for the negative value of f when reeling in, to render positive values for the two speed ratios. Combining Eqs. (6.33), (6.36) and (6.37) and solving for the nondimensional apparent wind speed leads to the following expression

$$\frac{v_\mathrm{a}}{v_\mathrm{w}} = \sqrt{1-\frac{f^2}{1+\frac{1}{E^2}}} - \frac{f}{\sqrt{1+E^2}}, \tag{6.38}$$

$$= \frac{\sqrt{1+E^2\,(1-f^2)}-f}{\sqrt{1+E^2}}. \tag{6.39}$$

While Eq. (6.31) describes the influence of the elevation angle and reeling speed on the apparent wind speed, Eq. (6.39) describes the influence of the lift-to-drag ratio and reeling speed. Although derived here for the reel-in phase with $f<0$, both equations are equally valid for the reel-out phase with $f>0$. Combining the two equations and solving for the lift-to-drag ratio gives

$$E = \frac{\sqrt{1-\cos^2\beta}}{\cos\beta - f} = \frac{\sin\beta}{\cos\beta - f}. \tag{6.40}$$

To maintain the steady-state descent of a massless kite with a given reel in speed and elevation angle, a lift-to-drag ratio according to Eq. (6.40) has to be enforced. For $f=0$, Eq. (6.40) reduces to the known result $E=\tan\beta$.

Combining Eqs. (6.23) and (6.39), we can further derive an expression for the elevation angle of a kite flying along a radial flight path, i.e., with $\lambda=0$, towards or away from the ground attachment point,

$$\cos\beta = \frac{\sqrt{1+E^2(1-f^2)}+fE^2}{1+E^2}. \tag{6.41}$$

Equation (6.39) gives rise to an important operational constraint for the steady-state retraction of a massless kite. Requiring that the radicand in the numerator is larger or equal to zero leads to the following minimum value for the reeling factor

$$f_\mathrm{min} = -\sqrt{1+\frac{1}{E^2}}. \tag{6.42}$$

By setting the square root in Eq. (6.41) to zero, we get the corresponding maximum elevation angle that the kite with a lift-to-drag ratio E can assume during steady-state flight operation with a reeling factor f.

$$\cos\beta_{\max} = \frac{f_{\min}E^2}{1+E^2}. \tag{6.43}$$

This operational limit shows that a very low lift-to-drag ratio is needed for fast reel-in. For $E \gg 1$ the minimum reeling factor is -1, while for $E = 1$ it only decreases to $-\sqrt{2}$. Since the tether force is relatively low during the reel-in phase, it can be assumed that the gravitational forces neglected in the above theory have a significant effect and decrease the limit further to below the theoretical value given by Eq. (6.42).

While the aerodynamic characteristics of fixed-wing kites can modulated rapidly to low and even negative values of the lift-to-drag ratio (close to zero and negative angle of attack), this is not possible with soft-wing kites. The actuation of this type of kite is slower and, for reasons of structural stability, restricted to a positive lift-to-drag ratio (positive angle of attack). Because of this, we implement the reel-in phase with a constant, prescribed lift-to-drag ratio E and a dependent elevation angle β. In this case, the nondimensional tether force and tractive power during the reel-in phase can be derived by inserting Eq. (6.39) into Eqs. (6.14) and (6.15)

$$\frac{F_\mathrm{t}}{qS} = C_\mathrm{L}\sqrt{1+\frac{1}{E^2}}\frac{\left(\sqrt{1+E^2\left(1-f^2\right)}-f\right)^2}{1+E^2}, \tag{6.44}$$

$$\frac{P}{P_\mathrm{w}S} = C_\mathrm{L}\sqrt{1+\frac{1}{E^2}}f\frac{\left(\sqrt{1+E^2\left(1-f^2\right)}-f\right)^2}{1+E^2}. \tag{6.45}$$

Compared to Eqs. (6.24) and (6.25), the above expressions miss the factor $1+E^2$, which, especially for $E \gg 1$ is reflecting the substantial amplification of the tether force and tractive power in the reel-out phase flying crosswind maneuvers.

Mechanical cycle power

Expressing the tether force during the reel-out phase by Eq. (6.24), and during the reel-in phase by Eq. (6.44), the net mechanical energy per cycle can be calculated with the known tether length change as

$$E_\mathrm{c} = E_\mathrm{o} + E_\mathrm{i} = \left[F_{\mathrm{t,o}} - F_{\mathrm{t,i}}\right]\left(r_{\max} - r_{\min}\right), \tag{6.46}$$

$$= qS\left[\gamma_\mathrm{o}\left(\cos\beta_\mathrm{o} - f_\mathrm{o}\right)^2 - \gamma_\mathrm{i}\frac{\left(\sqrt{1+E_\mathrm{i}^2\left(1-f_\mathrm{i}^2\right)}-f_\mathrm{i}\right)^2}{1+E_\mathrm{i}^2}\right]\left(r_{\max} - r_{\min}\right), \tag{6.47}$$

where the nondimensional aerodynamic force factors for the reel-out and reel-in phases are defined as

$$\gamma_\mathrm{o} = C_{\mathrm{L,o}} \sqrt{1 + \frac{1}{E_\mathrm{o}^2}} \left(1 + E_\mathrm{o}^2\right), \tag{6.48}$$

$$\gamma_\mathrm{i} = C_{\mathrm{L,i}} \sqrt{1 + \frac{1}{E_\mathrm{i}^2}}. \tag{6.49}$$

The average mechanical power is determined by dividing the net energy per cycle by the time duration of a cycle. Neglecting the transition phases, the cycle time is determined as the sum of the reel-in time $t_\mathrm{i} = t_3 - t_0$ and reel-out time $t_\mathrm{o} = t_5 - t_3$

$$t_\mathrm{c} = t_\mathrm{i} + t_\mathrm{o} = \frac{r_\mathrm{min} - r_\mathrm{max}}{f_\mathrm{i} v_\mathrm{w}} + \frac{r_\mathrm{max} - r_\mathrm{min}}{f_\mathrm{o} v_\mathrm{w}}, \tag{6.50}$$

$$= \frac{r_\mathrm{max} - r_\mathrm{min}}{v_\mathrm{w}} \frac{f_\mathrm{i} - f_\mathrm{o}}{f_\mathrm{i} f_\mathrm{o}}, \tag{6.51}$$

where t_0, t_3 and t_5 are defined as illustrated in Fig. 6.4. Defining a normalized average mechanical power or, in short, normalized cycle power, and substituting E_c by Eq. (6.47) and t_c by Eq. (6.51), leads to

$$p_\mathrm{c} = \frac{E_\mathrm{c}}{t_\mathrm{c} P_\mathrm{w} S \gamma_\mathrm{o}} = \left[(\cos\beta_\mathrm{o} - f_\mathrm{o})^2 - \frac{\gamma_\mathrm{i}}{\gamma_\mathrm{o}} \frac{\left(\sqrt{1 + E_\mathrm{i}^2 \left(1 - f_\mathrm{i}^2\right)} - f_\mathrm{i}\right)^2}{1 + E_\mathrm{i}^2} \right] \frac{f_\mathrm{i} f_\mathrm{o}}{f_\mathrm{i} - f_\mathrm{o}}, \tag{6.52}$$

with the aerodynamic force factors γ_o and γ_i defined in Eqs. (6.48) and (6.49), respectively. Since the generated energy generally is the dominating contribution to the cycle power, the force factor of the reel-out phase is used for the normalization, such that the ratio $\gamma_\mathrm{i}/\gamma_\mathrm{o}$ quantifies the relative effect of the consumed energy. From Eq. (6.52), the average cycle power can be evaluated as

$$P_\mathrm{c} = \frac{E_\mathrm{c}}{t_\mathrm{c}} = p_\mathrm{c} \gamma_\mathrm{o} P_\mathrm{w} S. \tag{6.53}$$

6.5 Performance optimization under operational constraints

Considering only the reel-out phase, the extreme value of the third-order polynomial in f on the right-hand side of Eq. (6.25) leads to the optimal reeling factor and corresponding optimal tractive power expressions (Luchsinger 2013)

$$f_\mathrm{opt} = \frac{1}{3} \cos\beta_\mathrm{o}, \tag{6.54}$$

$$\zeta_{\text{opt}} = \frac{4}{27}\cos^3\beta_{\text{o}}\gamma_{\text{o}}. \tag{6.55}$$

$$P_{\text{opt}} = \frac{4}{27}\cos^3\beta_{\text{o}}\gamma_{\text{o}}P_{\text{w}}S. \tag{6.56}$$

The expressions reflect the well-known dependencies of kite-based energy harvesting on key environmental, operational, and design parameters. The optimal reel-out speed is one-third of the wind speed when the tether is parallel to the ground, from where it progressively decreases with increasing elevation angle. As typical for wind energy converters, the tractive power P_{opt} increases with the cube of the wind speed stemming from the wind power density P_{w} given by Eq. (6.17). It decreases with the cubed cosine of the elevation angle, stressing the importance of maintaining an as low as possible elevation angle during reel out. To maximize the aerodynamic force factor γ_{o}, we note that for crosswind operation, the contribution of the tether to the total system drag sets a hard lower limit for the minimum system drag. For this reason, aerodynamic optimization is primarily about maximizing the lift coefficient of the kite.

Nevertheless, the theoretical performance projected by Eq. (6.56) is practically not achievable. On the one hand, the reel-in phase and other inherent conversion losses can not be neglected. On the other hand, any real system is subject to hardware limits that need to be considered when optimizing the system's operation. Important performance envelope borders originate from the maximum tensile force the tether can withstand and the maximum electrical power the generator can produce. The derivations so far have not considered these hardware limitations.

In the following, the maximum normalized cycle power is determined for three operational regimes. In the first regime, the wind speeds are sufficiently low that hardware limitations do not need to be considered. Accordingly, the cycle power is determined by optimizing the reeling speeds in both phases of the idealized cycle. In the second regime, the wind speeds have increased to a level where the maximum allowed tether force is reached in the reel-out phase. To keep the tether force at this limit, the reel-out speed is now increased with the wind speed, and only the reeling speed can be optimized to maximize the cycle power. In the third regime, the wind speeds have increased further to a level where also the maximum allowed generator power is reached. To comply with the joint force and power limits, the reel-out speed can not be increased any further. Instead, the aerodynamic properties of the kite or other operational parameters, such as the average elevation angle during reel-out, must be adjusted. As in the second regime, only the reel-in speed can be optimized to maximize the cycle power. The section is concluded by combining the three wind speed regimes within a single operation strategy.

Wind speed regime 1: unconstrained operation

At sufficiently low wind speeds, neither the maximum tether tension nor the maximum generator power are reached. With given set values β_{o} and E_{i} for the elevation angle during reel-out and the lift-to-drag ratio during reel-in, the normalized cycle

power given by Eq. (6.52) can be maximized by optimizing the reeling factors, f_o and f_i,

$$p_{\mathrm{c,opt}} = \max_{f_\mathrm{o},f_\mathrm{i}} \left\{ \left[(\cos\beta_\mathrm{o} - f_\mathrm{o})^2 - \frac{\gamma_\mathrm{i}}{\gamma_\mathrm{o}} \frac{\left(\sqrt{1+E_\mathrm{i}^2\left(1-f_\mathrm{i}^2\right)} - f_\mathrm{i}\right)^2}{1+E_\mathrm{i}^2} \right] \frac{f_\mathrm{i} f_\mathrm{o}}{f_\mathrm{i} - f_\mathrm{o}} \right\}. \tag{6.57}$$

For unconstrained operation, the aerodynamic force factors γ_i and γ_o are assumed to be constant.

Wind speed regime 2: constrained tether force

The first hardware limit that is generally encountered during the reel-out phase is the maximum allowed tether force, also denoted as rated or nominal tether force. Using Eqs. (6.16), (6.24) and (6.48), the tether force during the reel-out phase can be formulated as

$$F_\mathrm{t,o} = \frac{1}{2}\rho v_\mathrm{w}^2 S \gamma_\mathrm{o} \left(\cos\beta_\mathrm{o} - f_\mathrm{o}\right)^2, \tag{6.58}$$

which, when reaching the nominal force, evaluates to

$$F_\mathrm{t,n} = \frac{1}{2}\rho v_\mathrm{n,F}^2 S \gamma_\mathrm{o} \left(\cos\beta_\mathrm{o} - f_\mathrm{n,F}\right)^2, \tag{6.59}$$

where $v_\mathrm{n,F}$ and $f_\mathrm{n,F}$ are the wind speed and reeling factor at which this specific condition occurs. The nominal values $F_\mathrm{t,n}$, $v_\mathrm{n,F}$ and $f_\mathrm{n,F}$ are constant properties of a specific AWE system. An effective strategy to limit the tether force to the nominal value also for larger wind speeds is a controlled increase of the reeling speed. The reeling factor required to impose the constraint $F_\mathrm{t,o} = F_\mathrm{t,n}$ for $v_\mathrm{w} > v_\mathrm{n,F}$ can be derived by combining Eqs. (6.24) and (6.59) to

$$\frac{1}{2}\rho v_\mathrm{w}^2 S \gamma_\mathrm{o} \left(\cos\beta_\mathrm{o} - f_\mathrm{o}\right)^2 = \frac{1}{2}\rho v_\mathrm{n,F}^2 S \gamma_\mathrm{o} \left(\cos\beta_\mathrm{o} - f_\mathrm{n,F}\right)^2, \tag{6.60}$$

which, assuming a constant aerodynamic force factor γ_o and elevation angle β_o, leads to

$$f_\mathrm{o} = \frac{\cos\beta_\mathrm{o}\left(\mu_\mathrm{F} - 1\right) + f_\mathrm{n,F}}{\mu_\mathrm{F}}. \tag{6.61}$$

In the above expression, we introduced the nondimensional velocity parameter

$$\mu_\mathrm{F} = \frac{v_\mathrm{w}}{v_\mathrm{n,F}} > 1, \tag{6.62}$$

which quantifies how much the wind speed exceeds the nominal value. Equation (6.61) describes how, starting from $f_{\mathrm{n,F}}$ at $v_{\mathrm{n,F}}$, the reeling factor f_{o} increases with increasing wind speed v_{w} in regime 2. Since the tether force during the reel-in phase is much lower than during the reel-out phase, the reeling factor f_{i} can be varied freely to maximize the cycle power. The mechanical power during the reel-out phase is given by

$$P_{\mathrm{o}} = F_{\mathrm{t,n}} v_{\mathrm{w}} f_{\mathrm{n,F}}. \tag{6.63}$$

Substituting the constrained reeling factor given by Eq. (6.61) for f_{o} in Eq. (6.51) leads to the following expression for the cycle time

$$t_{\mathrm{c}} = \frac{r_{\max} - r_{\min}}{v_{\mathrm{w}}} \frac{\mu_{\mathrm{F}} f_{\mathrm{i}} - [(\mu_{\mathrm{F}} - 1)\cos\beta_{\mathrm{o}} + f_{\mathrm{n,F}}]}{f_{\mathrm{i}}\,[(\mu_{\mathrm{F}} - 1)\cos\beta_{\mathrm{o}} + f_{\mathrm{n,F}}]}. \tag{6.64}$$

The net mechanical energy per cycle can be defined similarly to Eqs. (6.46) and (6.47), but now calculating the nominal tether force $F_{\mathrm{t,n}}$ by substituting the constrained reeling factor given by Eq. (6.61) for f_{o} in Eq. (6.58). This results in the following expression

$$\begin{aligned} E_{\mathrm{c}} &= [F_{\mathrm{t,n}} - F_{\mathrm{t,i}}]\,(r_{\max} - r_{\min}), \\ &= qS\gamma_{\mathrm{o}} \left[\left(\frac{\cos\beta_{\mathrm{o}} - f_{\mathrm{n,F}}}{\mu_{\mathrm{F}}} \right)^2 - \frac{\gamma_{\mathrm{i}}}{\gamma_{\mathrm{o}}} \frac{\left(\sqrt{1 + E_{\mathrm{i}}^2 \left(1 - f_{\mathrm{i}}^2\right)} - f_{\mathrm{i}} \right)^2}{1 + E_{\mathrm{i}}^2} \right] (r_{\max} - r_{\min}). \end{aligned} \tag{6.65}$$

The factor $1/\mu_{\mathrm{F}}^2$ is responsible for a rapid decrease of the generated energy contribution when the wind speeds exceed the nominal value. The normalized cycle power can be formulated in analogy to Eq. (6.52). Substituting E_{c} by Eq. (6.65) and t_{c} by Eq. (6.64) gives

$$p_{\mathrm{c}} = \left[\left(\frac{\cos\beta_{\mathrm{o}} - f_{\mathrm{n,F}}}{\mu_{\mathrm{F}}} \right)^2 - \frac{\gamma_{\mathrm{i}}}{\gamma_{\mathrm{o}}} \frac{\left(\sqrt{1 + E_{\mathrm{i}}^2 \left(1 - f_{\mathrm{i}}^2\right)} - f_{\mathrm{i}} \right)^2}{1 + E_{\mathrm{i}}^2} \right] \frac{f_{\mathrm{i}}\,[(\mu_{\mathrm{F}} - 1)\cos\beta_{\mathrm{o}} + f_{\mathrm{n,F}}]}{\mu_{\mathrm{F}} f_{\mathrm{i}} - [(\mu_{\mathrm{F}} - 1)\cos\beta_{\mathrm{o}} + f_{\mathrm{n,F}}]}, \tag{6.66}$$

which can be maximized by optimizing the reeling factor f_{i},

$$p_{\mathrm{c,opt}} = \max_{f_\mathrm{i}} \left\{ \left[\left(\frac{\cos\beta_\mathrm{o} - f_\mathrm{n,F}}{\mu_\mathrm{F}} \right)^2 - \frac{\gamma_\mathrm{i}}{\gamma_\mathrm{o}} \frac{\left(\sqrt{1+E_\mathrm{i}^2\left(1-f_\mathrm{i}^2\right)} - f_\mathrm{i} \right)^2}{1+E_\mathrm{i}^2} \right] \frac{f_\mathrm{i}\left[(\mu_\mathrm{F}-1)\cos\beta_\mathrm{o} + f_\mathrm{n,F}\right]}{\mu_\mathrm{F} f_\mathrm{i} - \left[(\mu_\mathrm{F}-1)\cos\beta_\mathrm{o} + f_\mathrm{n,F}\right]} \right\}. \tag{6.67}$$

Because the tether force limit is maintained by modulating the reeling speed only, the aerodynamic force factors γ_i and γ_o are assumed to be constant, as was the case for unconstrained operation.

Wind speed regime 3: constrained tether force and generator power

With the tether force being constrained to the nominal value, the second hardware limit encountered at increasing wind speeds is the maximum allowed generator power, also denoted as rated or nominal generator power. Because the mechanical power is the product of tether force and reeling speed, the reeling speed can not be increased any further to compensate for higher wind speeds. Instead, the tether force is now limited by depowering the kite, adjusting its aerodynamic properties or other operational parameters. For example, Schelbergen et al. (2020) first increase the elevation angle during reel-out with increasing wind speeds, and only when this has reached a practical limit adjust also the aerodynamic properties. In the present work, we follow Luchsinger (2013) and adjust only the aerodynamic properties of the kite.

The nominal mechanical power of the generator can be evaluated as

$$P_\mathrm{n} = F_\mathrm{t,n} v_\mathrm{n,P} f_\mathrm{n,P}, \tag{6.68}$$

with the nominal tether force given by

$$F_\mathrm{t,n} = \frac{1}{2}\rho v_\mathrm{n,P}^2 S \gamma_\mathrm{o} \left(\cos\beta_\mathrm{o} - f_\mathrm{n,P}\right)^2, \tag{6.69}$$

where $v_\mathrm{n,P}$ and $f_\mathrm{n,P}$ represent the wind speed and reeling factor at which this specific nominal power value occurs. The parameters P_n, $v_\mathrm{n,P}$, and $f_\mathrm{n,P}$ are properties of the specific system. The product $v_\mathrm{n,P} f_\mathrm{n,P}$ is the nominal reeling speed which is kept constant throughout this wind speed regime until reaching the cut-out wind speed at which the operation is terminated. Enforcing a constant reeling speed for $v_\mathrm{w} > v_\mathrm{n,P}$ is expressed as

$$v_\mathrm{w} f_\mathrm{o} = v_\mathrm{n,P} f_\mathrm{n,P}, \tag{6.70}$$

which leads to

$$f_\mathrm{o} = \frac{f_\mathrm{n,P}}{\mu_\mathrm{P}}, \tag{6.71}$$

where we introduced the nondimensional velocity factor

$$\mu_\mathrm{P} = \frac{v_\mathrm{w}}{v_\mathrm{n,P}} > 1. \tag{6.72}$$

Equation (6.71) describes how, starting from $f_\mathrm{n,P}$ at $v_\mathrm{n,P}$, the reeling factor f_o decreases with increasing wind speed v_w in regime 3. To also keep the tether force at the nominal value, the force factor γ_o needs to be reduced for $v_\mathrm{w} > v_\mathrm{n,P}$. From Eq. (6.58) we derive the following relation

$$\gamma_\mathrm{o} = \frac{F_\mathrm{t,n}}{qS\left(\cos\beta_\mathrm{o} - f_\mathrm{o}\right)^2}, \tag{6.73}$$

which replaces Eq. (6.48) in wind speed regime 3 to calculate the force factor during reel-out.

The differentiation of wind speed regimes 2 and 3 is based on the assumption that the nominal force $F_\mathrm{t,n}$ is reached at a lower wind speed than the nominal power P_n, i.e. that $v_\mathrm{n,P} > v_\mathrm{n,F}$ (Luchsinger 2013; Schmehl et al. 2013). The values of nominal force and power depend on the specific design of the AWE system and are commonly a result of systematic trade-offs during the sizing of components.

Substituting the constrained reeling factor given by Eq. (6.71) for f_o in Eq. (6.51) leads to the following expression for the cycle time

$$t_\mathrm{c} = \frac{r_\mathrm{max} - r_\mathrm{min}}{v_\mathrm{w}} \frac{\mu_\mathrm{P} f_\mathrm{i} - f_\mathrm{n,P}}{f_\mathrm{i} f_\mathrm{n,P}}. \tag{6.74}$$

The net mechanical energy per cycle can be defined similarly to Eqs. (6.46) and (6.47), but now calulating the nominal tether force $F_\mathrm{t,n}$ by substituting the constrained reeling factor given by Eq. (6.71) for f_o in Eq. (6.58). This results in the following expression

$$\begin{aligned} E_\mathrm{c} &= \left[F_\mathrm{t,n} - F_\mathrm{t,i}\right]\left(r_\mathrm{max} - r_\mathrm{min}\right), \\ &= qS\gamma_\mathrm{o}\left[\left(\cos\beta_\mathrm{o} - \frac{f_\mathrm{n,P}}{\mu_\mathrm{P}}\right)^2 - \frac{\gamma_\mathrm{i}}{\gamma_\mathrm{o}}\frac{\left(\sqrt{1+E_\mathrm{i}^2\left(1-f_\mathrm{i}^2\right)} - f_\mathrm{i}\right)^2}{1+E_\mathrm{i}^2}\right]\left(r_\mathrm{max} - r_\mathrm{min}\right). \end{aligned} \tag{6.75}$$

The factor $1/\mu_\mathrm{P}^2$ is responsible for a rapid decrease in the generated energy contribution when the wind speeds exceed the nominal value. The normalized cycle power can be formulated in analogy to Eq. (6.52). Substituting E_c by Eq. (6.75) and t_c by Eq. (6.74) gives

$$p_\mathrm{c} = \left[\left(\cos\beta_\mathrm{o} - \frac{f_\mathrm{n,P}}{\mu_\mathrm{P}} \right)^2 - \frac{\gamma_\mathrm{i}}{\gamma_\mathrm{o}} \frac{\left(\sqrt{1+E_\mathrm{i}^2\left(1-f_\mathrm{i}^2\right)} - f_\mathrm{i} \right)^2}{1+E_\mathrm{i}^2} \right] \frac{f_\mathrm{i} f_\mathrm{n,P}}{\mu_\mathrm{P} f_\mathrm{i} - f_\mathrm{n,P}}, \tag{6.76}$$

which can be maximized by optimizing the reeling factor f_i,

$$p_\mathrm{c,opt} = \max_{f_\mathrm{i}} \left\{ \left[\left(\cos\beta_\mathrm{o} - \frac{f_\mathrm{n,P}}{\mu_\mathrm{P}} \right)^2 - \frac{\gamma_\mathrm{i}}{\gamma_\mathrm{o}} \frac{\left(\sqrt{1+E_\mathrm{i}^2\left(1-f_\mathrm{i}^2\right)} - f_\mathrm{i} \right)^2}{1+E_\mathrm{i}^2} \right] \frac{f_\mathrm{i} f_\mathrm{n,P}}{\mu_\mathrm{P} f_\mathrm{i} - f_\mathrm{n,P}} \right\}. \tag{6.77}$$

As mentioned above, the aerodynamic force factor γ_o is now modulated with the wind speed according to Eq. (6.73), while γ_i stays constant as given in Eq. (6.49).

Three-regime strategy

To determine the maximum cycle power over the entire operational wind speed range, three different wind speed regimes are distinguished:

1. Low wind speeds, $v_\mathrm{w,min} \leq v_\mathrm{w} < v_\mathrm{n,F}$.
2. Medium wind speeds, $v_\mathrm{n,F} \leq v_\mathrm{w} < v_\mathrm{n,P}$.
3. High wind speeds, $v_\mathrm{n,P} \leq v_\mathrm{w} < v_\mathrm{w,max}$.

The threshold wind speeds $v_\mathrm{n,F}$ and $v_\mathrm{n,P}$ are determined by stepping through the entire wind speed range starting from the cut-in wind speed $v_\mathrm{w,min}$ and ending at the cut-out wind speed $v_\mathrm{w,max}$. In the low wind speed regime, Eq. (6.57) is maximized by optimizing the nondimensional reeling speeds f_o and f_i. For each wind speed, the reel-out tether force $F_\mathrm{t,o}$ is computed from Eq. (6.58) and compared with the given nominal value $F_\mathrm{t,n}$ of the specific AWE system. Once $F_\mathrm{t,o}$ reaches $F_\mathrm{t,n}$, the system properties $v_\mathrm{n,F}$ and $f_\mathrm{n,F}$ are set to the current values of v_w and f_o.

In the following medium wind speed regime, the reel-out tether force $F_\mathrm{t,o}$ is kept at the nominal allowable value $F_\mathrm{t,n}$ by increasing f_o with the wind speed according to Eqs. (6.61) and (6.62). The maximum normalized cycle power given by Eq. (6.67) is determined by optimizing only f_i. For each wind speed, the reel-out mechanical power P_o is computed from Eq. (6.63) and compared with the nominal value P_n of the specific AWE system. Once P_o reaches P_n, the system properties $v_\mathrm{n,P}$ and $f_\mathrm{n,P}$ are set to the current values of v_w and f_o.

In the following high wind speed regime, the tether force $F_\mathrm{t,o}$ and mechanical power P_o are kept at their nominal allowable values $F_\mathrm{t,n}$ and P_n by jointly decreasing f_o with increasing wind speed according to Eqs. (6.71) and (6.72) and γ_o according

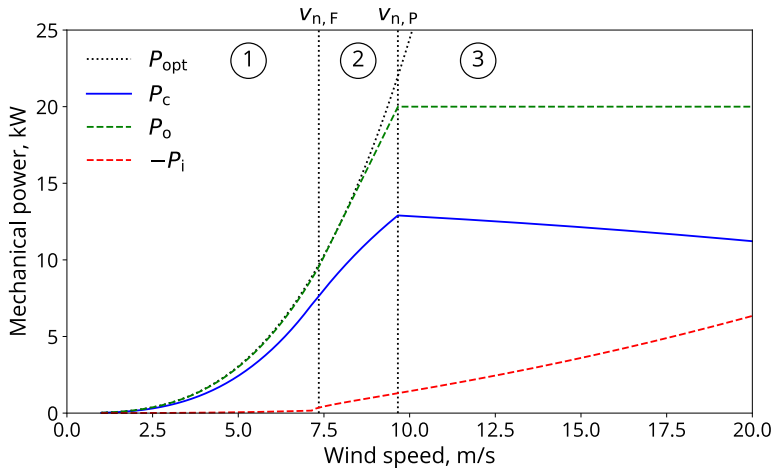

Fig. 6.7: Power curve in three wind speed regions: ① unconstrained operation, ② constrained tether force, and ③ constrained tether force and generator power.

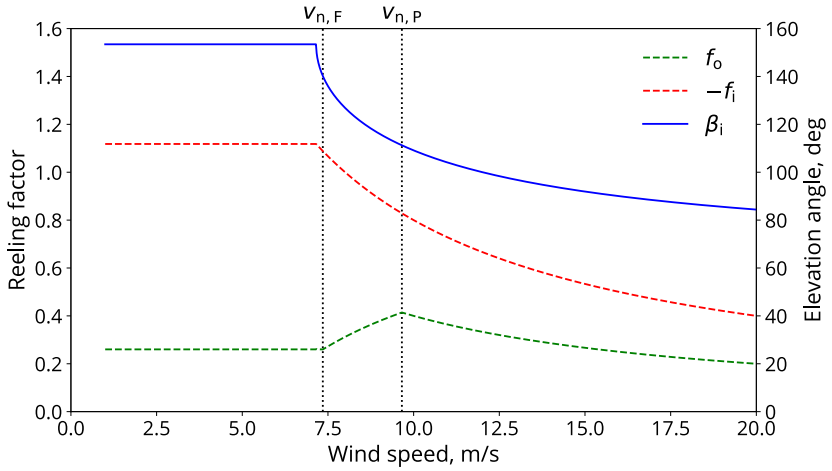

Fig. 6.8: Operational parameters in three wind speed regions.

to Eq. (6.73). The maximum normalized cycle power given by Eq. (6.77) is determined by optimizing only f_i.

The computed power curve of a representative AWE system is illustrated in Fig. 6.7, additional operational parameters in Fig. 6.8. The corresponding model input parameters are listed in Table 6.2. The drag contribution of the tether is only applied in the reel-out phase, where it has a significant effect. The performance of the system is evaluated in three different wind speed regimes, as outlined above,

Table 6.2: Model input parameters.

Parameter	**Value**
Atmospheric density, ρ (kg/m^3)	1.225
Elevation angle reel-out phase, β_o ($^\circ$)	25
Tether minimum reeling speed, $v_\mathrm{k,r,min}$ (m/s)	-8
Tether maximum reeling speed, $v_\mathrm{k,r,max}$ (m/s)	8
Tether minimum deployed length, r_min (m)	200
Tether maximum deployed length, r_max (m)	375
Kite planform area, S (m)	16.7
Kite lift coefficient reel-out phase, $C_\mathrm{L,o}$	1
Kite drag coefficient reel-out phase, $C_\mathrm{D,k,o}$	0.2
Kite lift coefficient reel-in phase, $C_\mathrm{L,i}$	0.14
Kite drag coefficient reel-in phase, $C_\mathrm{D,k,i}$	0.07
Tether drag coefficient, $C_\mathrm{D,t}$	1.1
Tether diameter, d_t (mm)	4
Nominal tether force, $F_\mathrm{t,n}$ (kN)	5
Nominal generator power, P_n, (kW)	20

not accounting for component efficiencies or any other losses. The aerodynamic characteristics of the kite are adopted from Van der Vlugt et al. (2013, Table 23.3).

The power curve exhibits the following behavior. Up to a wind speed of around 8.5 m/s, the reel-out power P_o closely tracks the optimal power P_opt defined by Eq. (6.56). Above this wind speed, P_o increases slower and, upon reaching the nominal wind speed, $v_\mathrm{n,P}$ levels out at the nominal value P_n. In wind speed regime 1, the magnitude of the reel-in power P_i is very low, practically zero. Shortly before reaching the transition to wind speed region 2, at $v_\mathrm{n,F} = 7.34$ m/s, P_i begins to increase continuously. As can be seen from Fig. 6.8, the very low reel-in power is caused by the very high elevation angle β_i in wind speed regime 1, which reduces the tether tension to a very low value. In fact, for the largest part in this regime, the reeling factor f_i is at its theoretical minimum value defined by Eq. (6.42), $f_\mathrm{min} = -1.118$. Accordingly, the elevation angle β_i is at its theoretical maximum value defined by Eq. (6.43), $\beta_\mathrm{max} = 153.4^\circ$.

The cycle power P_c reflects the combined effect of the two phase's contributions, reaching its maximum $P_\mathrm{c,max} = 12.9$ kW at the nominal wind speed $v_\mathrm{n,P} = 9.7$ m/s. Above this wind speed, P_c steadily decreases, which is largely an effect of the constant reel-out power while the magnitude of the reel-in power increases. Figure 6.8 indicates that in wind speed regimes 2 and 3, the magnitude of the reel-in factor and the reel-in elevation angle β_i steadily decrease. The reel-out factor f_o first increases in wind speed regime 2 and then decreases again in wind speed regime 3. This behavior of f_o illustrates the three-regime strategy discussed above. While the approach provides a consistent strategy to account for the machine limits of a real AWE system, the neglected mass of the kite leads to a clear overprediction of the reel-in elevation angle, resulting in very low losses during the reel-in phase. Ac-

counting for the mass of the kite in the reel-in phase will lead to a better prediction quality, but is out of the scope of the presented analysis.

The proposed performance model differs from Luchsinger (2013) in several aspects. Firstly, the elevation angle during the reel-out and reel-in phases is implemented consistently for all three wind speed regimes. A constant lift-to-drag ratio of the kite is prescribed for the reel-in phase, rendering the reel-in elevation angle dependent on the wind speed. In contrast to this, Luchsinger (2013) prescribed a constant reel-in elevation angle, rendering the lift-to-drag ratio dependent on the wind speed. While this is a reasonable approach for modeling fixed-wing kites, which can operate at negative and positive angles of attack, it is not feasible for soft-wing kites, which, for stability reasons, require a safe distance from negative angles of attack. The overall advantage of the proposed performance model and optimization procedure is the low computational cost.

6.6 Additional power conversion losses

So far, we have only considered the conversion of wind energy into mechanical net power. However, the conversion of mechanical into electrical net power via a cyclic process involving energy production, temporary storage, and consumption entails additional losses. These depend on the design and specification of the ground station and the operating conditions. We adopt the approach of Fechner and Schmehl (2013) to account for the conversion efficiencies of the alternating generator and motor modes. Other losses caused by the charging and discharging of the integrated battery/capacitor module, auxiliary drives and the thermal control are neglected in the present ground station analysis, for the purposed of simplicity. Further details about the ground station analysis are available in Corte Vargas et al. (2020).

Generator efficiency

According to Fechner and Schmehl (2013), assuming an identical, constant efficiency for generator and motor modes overestimates the overall conversion efficiency. Instead, they recommended modeling the component efficiencies as functions of the rotational speed of the drum and the applied torque.

The efficiency of the electrical machine in generator mode is defined as the ratio of electrical to mechanical power during the reel-out phase,

$$\eta_{\mathrm{e,o}} = \frac{P_{\mathrm{e,o}}}{P_{\mathrm{o}}}, \tag{6.78}$$

where

$$P_{\mathrm{o}} = F_{\mathrm{t,o}} v_{\mathrm{w}} f_{\mathrm{o}}. \tag{6.79}$$

The electrical power can also be evaluated by subtracting the conversion losses from the mechanical power,

$$P_{\mathrm{e,o}} = P_{\mathrm{o}} - L_{\mathrm{e,o}} - \tau_{\mathrm{f,o}}\omega_{\mathrm{o}}, \tag{6.80}$$

where $L_{\mathrm{e,o}}$ represents the electrical losses associated with current flow and generator resistance, and $\tau_{\mathrm{f,o}}\omega_{\mathrm{o}}$ the friction losses caused by the rotation of the drum with the angular velocity ω_{o} against the friction torque $\tau_{\mathrm{f,o}}$. The reel-out speed of the tether and the angular velocity of the drum are coupled by the kinematic relation

$$v_{\mathrm{w}} f_{\mathrm{o}} = r_{\mathrm{d}}\omega_{\mathrm{o}}, \tag{6.81}$$

where r_{d} is the drum radius. The electrical losses are calculated from

$$L_{\mathrm{e,o}} = 3R_{\mathrm{g}}I_{\mathrm{o}}^2 k, \tag{6.82}$$

where I_{o} denotes the electrical current, R_{g} the stage resistance, and k a constant factor accounting for other not explicitly modeled machine losses. The formulation of Eq. (6.82) implies $k \geq 1$. The electrical current is computed as

$$I_{\mathrm{o}} = \tau_{\mathrm{g}} c_{\mathrm{g}}, \tag{6.83}$$

where τ_{g} is the effective generator torque and c_{g} the generator constant. Assuming a quasi-steady rotation of the drum during the reel-out phase, the effective generator torque can be defined as

$$\tau_{\mathrm{g}} = F_{\mathrm{t,o}} r_{\mathrm{d}} - \tau_{\mathrm{f,o}}. \tag{6.84}$$

The friction torque $\tau_{\mathrm{f,o}}$ in Eqs. (6.80) and (6.84) can be modeled as an assembly of static and dynamic, velocity-dependent contributions

$$\tau_{\mathrm{f,o}} = \tau_{\mathrm{c}} + c_{\mathrm{v,f}} r_{\mathrm{d}}\omega_{\mathrm{o}}, \tag{6.85}$$

where τ_{c} is the static friction torque, and $c_{v,f}$ the dynamic friction coefficient.

Motor efficiency

The efficiency of the electrical machine in motor mode is derived along the same lines, with the difference that electrical energy is now used to perform work against the aerodynamic forces acting on the kite. For this reason, the electrical efficiency in motor mode is defined as the ratio of mechanical to electrical power,

$$\eta_{\mathrm{e,i}} = \frac{P_{\mathrm{i}}}{P_{\mathrm{e,i}}}, \tag{6.86}$$

where

$$P_{\mathrm{i}} = F_{\mathrm{t,i}} v_{\mathrm{w}} f_{\mathrm{i}}. \tag{6.87}$$

Similar to Eq. (6.80), the electrical power can be evaluated by subtracting the conversion losses from the mechanical power,

$$P_{\mathrm{e,i}} = P_{\mathrm{i}} - L_{\mathrm{e,i}} - \tau_{\mathrm{f,i}}\omega_{\mathrm{i}}. \tag{6.88}$$

During reel-in, P_{i} and $P_{\mathrm{e,i}}$ are both negative, with $P_{\mathrm{e,i}} < P_{\mathrm{i}}$. Both loss contributions, $L_{\mathrm{e,i}}$ and $\tau_{\mathrm{f,i}}\omega_{\mathrm{i}}$ are positive. Similar to Eq. (6.81), the reel-in speed of the tether and the angular velocity of the drum are coupled by the kinematic relation

$$v_{\mathrm{w}} f_{\mathrm{i}} = r_{\mathrm{d}}\omega_{\mathrm{i}}. \tag{6.89}$$

Because f_{i} is negative, also ω_{i} is negative, and, because $\tau_{\mathrm{f,i}}\omega_{\mathrm{i}}$ is positive, $\tau_{\mathrm{f,i}}$ is negative. Similar to Eq. (6.82), the electrical conversion losses are evaluated as a function of the passing current and phase resistance,

$$L_{\mathrm{e,i}} = 3R_{\mathrm{m}}I_{\mathrm{i}}^2 k, \tag{6.90}$$

where the electrical current I_{i} is evaluated as the product of the motor constant c_{m} and the effective motor torque τ_{m} required to drive the drum. As for the derivation of Eq. (6.84), we assume a quasi-steady rotation of the drum during the reel-in phase, defining the effective motor torque as

$$\tau_{\mathrm{m}} = F_{\mathrm{t,i}} r_{\mathrm{d}} - \tau_{\mathrm{f,i}}. \tag{6.91}$$

With τ_{m} and $F_{\mathrm{t,i}} r_{\mathrm{d}}$ both positive and $\tau_{\mathrm{f,i}}$ negative, we can see that $\tau_{\mathrm{m}} > F_{\mathrm{t,i}} r_{\mathrm{d}}$ because the motor torque needs to overcome the additional friction torque $\tau_{\mathrm{f,i}}$ during reel-in.

6.7 Electrical power output

The electrical net power production for a certain wind speed and atmospheric density is calculated by applying the efficiencies derived in Sect. 6.6 to the energy conversions during the reel-in and reel-out phases. To determine the energy produced over an entire day the probability at which the different wind speeds occur during this day need to be factored in. This is the step in the analysis where the wind resource assessment is combined with the performance model.

Electrical cycle power

Similar to the net mechanical energy per pumping cycle presented in Eq. (6.46), we can define the net electrical energy per cycle as

$$E_{\mathrm{e,c}} = E_{\mathrm{e,o}} + E_{\mathrm{e,i}}. \tag{6.92}$$

To determine the electrical cycle power we introduce the conversion efficiencies defined in Eqs. (6.78) and (6.86),

$$P_{\mathrm{e,c}} = \frac{E_{\mathrm{e,o}} + E_{\mathrm{e,i}}}{t_o + t_i}, \tag{6.93}$$

$$= \frac{1}{t_\mathrm{i} + t_\mathrm{o}} \left(t_\mathrm{o} \eta_{\mathrm{e,o}} P_\mathrm{o} + t_\mathrm{i} \frac{1}{\eta_{\mathrm{e,i}}} P_\mathrm{i} \right). \tag{6.94}$$

It is important to note that, in the present study, the additional power conversion losses are taken into account only after determining the optimal mechanical cycle power $P_{\mathrm{c,opt}}$, as described in Sect. 6.5. This means the optimal point of operation maximizing the electrical cycle power can deviate from the purely mechanically determined optimum. In the frame of the presented feasibility analysis we assume that this deviation is not significant. For a more refined analysis, this should however be taken into account.

Daily energy production

The probability distribution of the wind speeds over a day can generally be described by a Weibull distribution function, which we use in a discretized form. Following the three-regime strategy presented in Sect. 6.5, the average electrical power per day is evaluated by integrating the product of electrical cycle power and the corresponding wind speed probability over the three consecutive wind speed ranges

$$\begin{aligned} P_{\mathrm{e,d}} = &\int_{v_{\mathrm{w,min}}}^{v_{\mathrm{n,F}}} P_{\mathrm{e,c}}(v) g_\mathrm{w}(v)\, dv \\ &+ \int_{v_{\mathrm{n,F}}}^{v_{\mathrm{n,P}}} P_{\mathrm{e,c}}(v) g_\mathrm{w}(v)\, dv + \int_{v_{\mathrm{n,P}}}^{v_{\mathrm{w,max}}} P_{\mathrm{e,c}}(v) g_\mathrm{w}(v)\, dv. \end{aligned} \tag{6.95}$$

The lower bound of the first integral, $v_{\mathrm{w,min}}$, is the cut-in wind speed at which the harvesting operation starts, while the upper bound of the last integral, $v_{\mathrm{w,max}}$, is the cut-out wind speed at which the harvesting operation is discontinued.

With the average electrical power per day, $P_{\mathrm{e,d}}$, and the time duration of the day, t_d the daily energy production of the AWE system is given by

$$E_{\mathrm{e,d}} = t_\mathrm{d} P_{\mathrm{e,d}}. \tag{6.96}$$

6.8 Conclusions

This work provides a performance model for the pumping cycle operation of AWE systems. The model uses two representative quasi-steady flight states to discretize the pumping cycle, implementing a constant average elevation angle for the reel-out phase and a variable elevation angle for the reel-in phase. The model is used

for systematic optimization of the operational parameters, to maximize the energy output for specific wind resource conditions and system specifications. To further improve the model in future work, it is suggested to account for the effect of gravity on the kite, which is particularly important during the reel-in phase. An additional measure to further increase the fidelity of the model is a numerical integration of the reel-in trajectory of the kite. This is particularly important for soft-kite systems with limited options to control the lift-to-drag ratio of the wing.

Data availability The Python code used for this study is available from https://github.com/awecourse/resources/.

Acknowledgements The author would like to thank Rafael Dux for providing a solution for an error in the theory for wind speed regime 3.

List of Abbreviations and Symbols

AEP Annual energy production
AWE Airborne wind energy
KCU Kite control unit

References

Corte Vargas F, Géczi M, Heidweiller S, Kempers MX, Klootwijk BJ, Marion F. Mordasov D van, Ouroumova LH, Terwindt EN and Witte D (2020) Arcadian Renewable Energy System: Renewable Energy for Mars Habitat. B.Sc. Thesis. Delft University of Technology. http://resolver.tudelft.nl/uuid:93c343e5-ee79-4320-98a3-949d3e9c407d. Accessed 3 Aug 2022.

Diehl M (2013) Airborne Wind Energy: Basic Concepts and Physical Foundations. In: Ahrens U, Diehl M and Schmehl R (eds) Airborne Wind Energy. Green Energy and Technology. Springer, Berlin Heidelberg. Chap. 1, pp 3–22. https://doi.org/10.1007/978-3-642-39965-7_1.

Fechner U and Schmehl R (2013) Model-Based Efficiency Analysis of Wind Power Conversion by a Pumping Kite Power System. In: Ahrens U, Diehl M and Schmehl R (eds) Airborne Wind Energy. Green Energy and Technology. Springer, Berlin Heidelberg. Chap. 14, pp 249–269. https://doi.org/10.1007/978-3-642-39965-7_10.

Fechner U (232016) A Methodology for the Design of Kite-Power Control Systems. Ph.D. Thesis. Delft University of Technology. https://doi.org/10.4233/uuid:85efaf4c-9dce-4111-bc91-7171b9da4b77.

Fechner U and Schmehl R (2018) Flight Path Planning in a Turbulent Wind Environment. In: Schmehl R (ed) Airborne Wind Energy – Advances in Technology

Development and Research. Green Energy and Technology. Springer, Singapore. Chap. 15, pp 361–390. https://doi.org/10.1007/978-981-10-1947-0_15.

Hagen L van, Petrick K, Wilhelm S and Schmehl R (2023) Life-Cycle Assessment of a Multi-Megawatt Airborne Wind Energy System. Energies 16(4): 1750. https://doi.org/10.3390/en16041750.

Loyd ML (1980) Crosswind kite power. Journal of Energy 4(3): 106–111. https://doi.org/10.2514/3.48021.

Luchsinger RH (2013) Pumping Cycle Kite Power. In: Ahrens U, Diehl M and Schmehl R (eds) Airborne Wind Energy. Green Energy and Technology. Springer, Berlin Heidelberg. Chap. 3, pp 47–64. https://doi.org/10.1007/978-3-642-39965-7_3.

Salma V, Friedl F and Schmehl R (102019) Improving Reliability and Safety of Airborne Wind Energy Systems. Wind Energy 23(2): 340–356. https://doi.org/10.1002/we.2433.

Schelbergen M, Kalverla PC, Schmehl R and Watson SJ (2020) Clustering wind profile shapes to estimate airborne wind energy production. Wind Energy Science 5(3): 1097–1120. https://doi.org/10.5194/wes-5-1097-2020.

Schmehl R, Noom M and Vlugt R van der (2013) Traction Power Generation with Tethered Wings. In: Ahrens U, Diehl M and Schmehl R (eds) Airborne Wind Energy. Green Energy and Technology. Springer, Berlin Heidelberg. Chap. 2, pp 23–45. https://doi.org/10.1007/978-3-642-39965-7_2.

Schmehl R, Rodriguez M, Ouroumova L and Gaunaa M (2024) Airborne Wind Energy for Martian Habitats. In: Cervone A, Bier H and Makaya A (eds) Adaptive on- and off-Earth Environments. Adaptive Environments. Springer Nature, Cham. Chap. 7, pp 145–197. https://doi.org/10.1007/978-3-031-50081-7_7.

Terink EJ (2009) Kiteplane Flight Dynamics. M.Sc. Thesis. Delft University of Technology. http://resolver.tudelft.nl/uuid:3e777823-ef53-4ac7-b246-cd7ff7b39487. Accessed 15 Jun 2023.

Van der Vlugt R, Bley A, Schmehl R and Noom M (2019) Quasi-Steady Model of a Pumping Kite Power System. Renewable Energy 131: 83–99. https://doi.org/10.1016/j.renene.2018.07.023.

Van der Vlugt R, Peschel J and Schmehl R (2013) Design and Experimental Characterization of a Pumping Kite Power System. In: Ahrens U, Diehl M and Schmehl R (eds) Airborne Wind Energy. Green Energy and Technology. Springer, Berlin Heidelberg. Chap. 23, pp 403–425. https://doi.org/10.1007/978-3-642-39965-7_23.

Vander Lind D (2013) Analysis and Flight Test Validation of High Performance Airborne Wind Turbines. In: Ahrens U, Diehl M and Schmehl R (eds) Airborne Wind Energy. Green Energy and Technology. Springer, Berlin Heidelberg. Chap. 28, pp 473–490. https://doi.org/10.1007/978-3-642-39965-7_28.